New Compound Fractional Sliding Mode Control and Super-Twisting Control of a MEMS Gyroscope

Mehran Rahmani
The Polytechnic School,
Ira Fulton School of Engineering,
Arizona State University,
Mesa, AZ 85212
e-mail: mrahma61@asu.edu

Sangram Redkar[1]
The Polytechnic School,
Ira Fulton School of Engineering,
Arizona State University,
Mesa, AZ 85212
e-mail: sredkar@asu.edu

This research proposes a new compound fractional sliding mode control (FOSMC) and super-twisting control (FOSMC + STC) to control a microelectromechanical systems gyroscope. A new sliding mode surface has been defined to design the proposed new sliding mode controller. The main advantages of a FOSMC are its high tracking performance and robustness against external perturbation, but creating a chattering phenomenon is its main drawback. By applying a super-twisting control (STC) method with FOSMC, the chattering phenomenon is eliminated, the singularity problem is solved, and systems robustness has significantly improved. Simulation results validate the effectiveness of the proposed control approach. [DOI: 10.1115/1.4055878]

Keywords: chattering reduction, compound control, fractional sliding mode control, MEMS gyroscope, super-twisting control, control applications, emerging control approaches

1 Introduction

Microelectromechanical systems (MEMS) gyroscopes are usually used to measure angular velocity, which can be utilized in different applications such as biosystems and control stabilization. However, the MEMS gyroscope performance degrades due to the frequency of oscillation mismatch between the two vibrating axes created by external disturbances and time-varying parameters [1]. Therefore, the best performance for the MEMS gyroscope can be obtained by designing an appropriate control method.

Fractional calculus has been widely used for many years. It provides more accurate results for different systems, such as in Robotics and control systems engineering [2]. The fractional-order theory has been applied in various structures because of its ease of modeling dynamics and nonlinear control. Fractional sliding mode control (FOSMC) is a powerful tool in control systems engineering. It is robust against external disturbances and has high tracking performance [3]. Yang and Liu considered the FOSMCto control a hyperchaotic structure [4]. Gao and Liao presented integral sliding mode control to enhance the robustness of FOSMC [5]. Balochian used variable structure control for an individual polytopic system with a fractional-order operator. A specific feedback law is considered by proposing a sliding surface with a fractional-order operator [6]. Rabah et al. provided a novel technique of FOSMC to guarantee the asymptotic stability of fractional systems [7]. Shah and Mehta described Thiran's delay estimation scheme to compensate the controller for fractional actuator delay, considering the real-time networked medium and packet loss situation [8]. Sun and Mah, to achieve high convergence precision, applied a fractional integral sliding mode control for tracking control of the linear motor. Experimental results validated that the proposed control law has high tracking performance compared to conventional sliding mode control [9]. Wang et al. proposed a new fractional-order nonsingular terminal sliding mode control. Due to the fractional-order nonsingular terminal sliding mode control and fast terminal sliding mode controller, the proposed controller guarantees fast convergence and high tracking performance [10]. Aghababa presented a new fractional hierarchical terminal sliding mode surface, in which its finite-time convergence to the origin is demonstrated. A robust sliding mode switching control method is proposed to guarantee the fractional Lyapunov stability theory and sliding mode control technique in Ref. [11]. Wang et al. implemented a novel sliding mode controller for an active vehicle suspension system to suppress external noise that acts on that system [12]. Based on the previous research, FOSMC can be used as a robust control method in different systems [13–15], but its main drawback is creating a chattering phenomenon.

Super-twisting control (STC) is a technique that can be used in control systems. It overcomes disturbances of super-twisting control [16]. Jeong et al. designed a robust super-twisting sliding mode control that guarantees a high tracking trajectory of a robotic system. To satisfy the properties of a conventional sliding mode control, a super-twisting sliding mode surface is designed for obtaining the transient and steady-state time performances of the position of the robotic manipulator [17]. Chuei et al. described a super-twisting observer-based repetitive control, which overcomes aperiodic disturbances [18]. Zargham and Mazinan applied a super-twisting sliding mode control method to control the wind turbine system. However, conventional sliding mode control cannot guarantee closed-loop performance against external perturbations; due to this drawback, an STC technique is used for rapid response and high accuracy in chattering reduction [19]. Zhao et al. proposed a nonsingular terminal sliding mode control based on the STC method to eliminate the chattering phenomenon and avoid the singularity problem [20]. Lu and Xia addressed a new adaptive super-twisting algorithm for controlling rigid spacecraft. The applied controller is anti-singularity and anti-chattering when encountered with external disturbances [21]. Evangelista et al. used modified STC, which improves the system's robustness in external perturbations acting on a wind turbine shaft [22]. Becerra et al. proposed an STC which guarantees continuous control inputs and enhances robustness properties [23]. Salgado et al. introduced a discrete-time super-twisting algorithm to solve the problems of control and state estimation [24]. As a result of considered studies, STC can be a vital tool in control systems. It has some advantages, such as improving the robustness of control systems, removing controller singularity, and eliminating the chattering phenomenon.

[1]Corresponding author.

Manuscript received July 18, 2022; final manuscript received September 29, 2022; published online November 2, 2022. Assoc. Editor: G. M. Clayton.

The contributions of this research are as follows:

(1) Propose a new fractional sliding mode surface for use in the FOSMC to suppress the external perturbations.
(2) A new compound FOSMC and STC is proposed, in which the STC controller will calculate an error value and apply a correction value to the system. Therefore, the proposed compound control method, reduces the oscillation, increases tracking performance, and reduces the tracking error.

Section 2 presents the dynamic modeling of a MEMS gyroscope. In Sec. 3, the FOSMC is described. Section 4, compound FOSMC + STC has been delineated. Section 5 presents simulation results. Section 6 concludes the paper.

2 Dynamics of MEMS Gyroscope

A z-axis MEMS gyroscope is shown in Fig. 1. The conventional MEMS vibratory gyroscope consists of a proof mass (m) suspended by springs, where x and y are the coordinates of the proof mass with respect to the gyro frame in a cartesian coordinate system, sensing mechanisms, and an electrostatic actuation for forcing an oscillatory motion and velocity of the proof mass and sensing the position. $\Omega_{x,y,z}$ are the angular rate components along each axis of the gyro frame. The frame where the proof mass is mounted moves with a constant velocity, and the gyroscope rotates at a slowly changing angular velocity Ω_z. The centrifugal forces m $\Omega_z^2 x$ and m $\Omega_z^2 y$ are assumed to be negligible because of small displacements. The Coriolis force is generated perpendicular to the drive and rotational axes [25].

The dynamics equations of the gyroscope are given by

$$m\ddot{x} + d_{xx}^*\dot{x} + d_{xy}^*\dot{y} + k_{xx}^* x + k_{xy}^* y = u_x^* + 2m\Omega_z^*\dot{y} \tag{1}$$

$$m\ddot{y} + d_{xy}^*\dot{y} + d_{yy}^*\dot{y} + k_{xy}^* x + k_{yy}^* y = u_y^* - 2m\Omega_z^*\dot{x} \tag{2}$$

The origin for x and y coordinates is at the center of the proof mass without force employed. Fabrication imperfections will affect the asymmetric spring and damping terms, k_{xy}^* and d_{xy}^*, respectively. The stiffness and damping terms are given by k_{xx}^*, k_{yy}^*, d_{xx}^*, and d_{yy}^*

The stiffness and damping terms may vary slightly from nominal values [1,25]. However, the magnitude of the proof mass m can be obtained precisely.

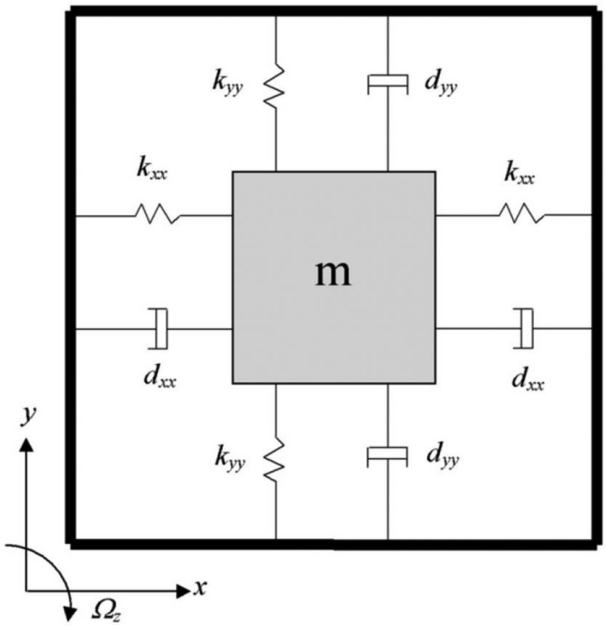

Fig. 1 Structure of MEMS gyroscope

The u_x^* and u_y^* are the control forces in the x- and y-directions. Dividing gyroscope dynamics (Eqs. (1) and (2)) by the reference mass results in the following vector forms:

$$\ddot{q}^* + \frac{D^*}{m}\dot{q}^* + \frac{K_a}{m}q^* = \frac{u^*}{m} - 2\Omega^*\dot{q}^* \tag{3}$$

where

$$q^* = \begin{bmatrix} x^* \\ y^* \end{bmatrix}, \quad u = \begin{bmatrix} u_x^* \\ u_y^* \end{bmatrix}, \quad \Omega^* = \begin{bmatrix} 0 & -\Omega_z^* \\ \Omega_z^* & 0 \end{bmatrix}$$

$$D^* = \begin{bmatrix} d_{xx}^* & d_{xy}^* \\ d_{xy}^* & d_{yy}^* \end{bmatrix}, \quad K_a = \begin{bmatrix} k_{xx}^* & k_{xy}^* \\ k_{xy}^* & k_{yy}^* \end{bmatrix}$$

The final form of the non-dimensional equation of motion as follows:

$$\frac{\ddot{q}^*}{q_0} + \frac{D^*}{m\omega_0}\frac{\dot{q}^*}{q_0} + \frac{K_a}{m\omega_0^2}\frac{q^*}{q_0} = \frac{u^*}{m\omega_0^2 q_0} - 2\frac{\Omega^*}{\omega_0}\frac{\dot{q}^*}{q_0} \tag{4}$$

we determine a set of new parameters as follows:

$$q = \frac{q^*}{q_0}, \quad d_{xy} = \frac{d_{xy}^*}{m\omega_0}, \quad \Omega_z = \frac{\Omega_z^*}{\omega_0} \tag{5}$$

$$u = \frac{u_x^*}{m\omega_0^2 q_0}, \quad u_y = \frac{u_y^*}{m\omega_0^2 q_0} \tag{6}$$

$$\omega_x = \sqrt{\frac{k_{xx}}{m\omega_0^2}}, \quad \omega_y = \sqrt{\frac{k_{yy}}{m\omega_0^2}}, \quad \omega_{xy} = \frac{k_{xy}}{m\omega_0^2} \tag{7}$$

$$\ddot{q} + D\dot{q} + K_b q = u - 2\Omega\dot{q} \tag{8}$$

where

$$q = \begin{bmatrix} x \\ y \end{bmatrix}, \quad u = \begin{bmatrix} u_x \\ u_y \end{bmatrix}, \quad \Omega = \begin{bmatrix} 0 & -\Omega_z \\ \Omega_z & 0 \end{bmatrix}$$

$$D = \begin{bmatrix} d_{xx} & d_{xy} \\ d_{xy} & d_{yy} \end{bmatrix}, \quad K_b = \begin{bmatrix} \omega_x^2 & \omega_{xy} \\ \omega_{xy} & \omega_y^2 \end{bmatrix}$$

Equation (8) can be rearranged as follows:

$$\ddot{q} = -(D + 2\Omega)\dot{q} - K_b q + u + E \tag{9}$$

where E is an external disturbance. Since the disturbance is considered unknown, the model from Eq. (9) used to generate the control signal must be modified by setting $E = 0$

$$\ddot{q} = -M\dot{q} - Nq + u \tag{10}$$

where $M = (D + 2\Omega)$ and $N = K_b$.

3 New Fractional Sliding Mode Control

Selecting a fractional sliding mode surface is the central part of FOSMC design. The fractional derivative and integral order in sliding mode surface provide the flexibility of having fractional type of error in controller design. The best performance will be obtained if a fractional sliding mode surface is chosen correctly. The fractional sliding mode surface can be selected as follows:

$$s(t) = \dot{e}(t) + \alpha D^{\mu-1}e(t) + \beta D^{\mu-2}e(t) + \gamma\int_0^t e(\tau)^{\frac{r}{m}}d\tau \tag{11}$$

where r, m, α, β, and γ are positive constants, and D is a fractional-order operator ($D = d/dt$, and $\mu > 2$). The fractional-order

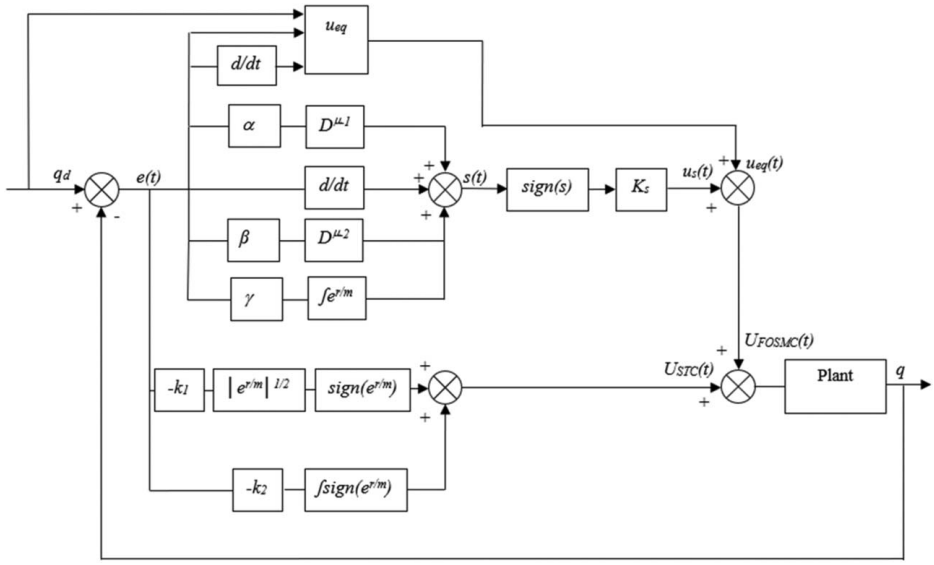

Fig. 2 Block diagram of novel control system

operator type is Grunwald–Letnikov. The tracking error can be shown as

$$e(t) = q - q_d \tag{12}$$

The derivative of the fractional sliding mode surface is

$$\begin{aligned}\dot{s}(t) &= \ddot{e}(t) + \alpha D^{\mu} e(t) + \beta D^{\mu-1} e(t) + \gamma e(t)^{\frac{r}{m}} \\ &= \ddot{q} - \ddot{q}_d + \alpha D^{\mu} e(t) + \beta D^{\mu-1} e(t) + \gamma e(t)^{\frac{r}{m}} \\ &= -M\dot{q} - Nq + u - \ddot{q}_d + \alpha D^{\mu} e(t) + \beta D^{\mu-1} e(t) + \gamma e(t)^{\frac{r}{m}}\end{aligned} \tag{13}$$

Equivalent control u_{eq} can be obtained by setting $\dot{s}(t) = 0$.

$$u_{eq}(t) = M\dot{q} + Nq + \ddot{q}_d - \alpha D^{\mu} e(t) - \beta D^{\mu-1} e(t) - \gamma e(t)^{\frac{r}{m}} \tag{14}$$

The FOSMC can be shown as

$$\begin{aligned}u_{FOSMC}(t) = u_{eq}(t) + u_s(t) = M\dot{q} + Nq + \ddot{q}_d - \alpha D^{\mu} e(t) - \beta D^{\mu-1} e(t) \\ - \gamma e(t)^{\frac{r}{m}} - K_s s\end{aligned} \tag{15}$$

The equivalent control cannot compensate for external perturbation and unmodeled dynamic uncertainties. A reaching control law can be designed to remove those problems as $u_s(t)$, which can be defined as:

$$u_s(t) = -K_s \text{sign}(s) \tag{16}$$

where K_s is a positive constant.

Considering the following Lyapunov function candidate (V), continuous and non-negative [26–28].

$$V = \frac{1}{2} s^T s \tag{17}$$

The time derivative of V yields

$$\dot{V} = s^T \dot{s} = s^T (-M\dot{q} - Nq + u(t) - \ddot{q}_d + \alpha D^{\mu} e(t) + \beta D^{\mu-1} e(t) + \gamma e(t)^{\frac{r}{m}}) \tag{18}$$

By substituting Eqs. (15) into (18) generates

$$\begin{aligned}\dot{V} = s^T \dot{s} = s^T (&-M\dot{q} - Nq + M\dot{q} + Nq + \ddot{q}_d - \alpha D^{\mu} e(t) \\ &- \beta D^{\mu-1} e(t) - \gamma e(t)^{\frac{r}{m}} \\ &- K_s s - \ddot{q}_d + \alpha D^{\mu} e(t) + \beta D^{\mu-1} e(t) + \gamma e(t)^{\frac{r}{m}})\end{aligned} \tag{19}$$

Simplifying Eq. (19) results in

$$\dot{V} = s^T (-K_s \text{sign}(s)) \tag{20}$$

Therefore, Eq. (20) can be expressed as

$$\dot{V} = -K_s s^T \text{sign}(s) \tag{21}$$

Equation (21) shows that $\dot{V} < 0$, which expressed that the proposed control law is stable.

4 New Compound Fractional Sliding Mode Control and Super-Twisting Control

Fractional sliding mode control is one of the techniques that can enhance the robustness of the control system and improve tracking performance. As discussed before, its main drawback is creating a chattering phenomenon. However, STC can be used in conjunction with FOSMC to minimize chattering of the system, improve trajectory tracking, and remove singularity problems. By combining both FOSMC and STC, a better control method will be obtained, combining both controllers' benefits. The Block diagram of the proposed controller is illustrated in Fig. 2. The compound control law can be defined as

$$u(t) = u_{FOSMC}(t) + u_{STC}(t) \tag{22}$$

where $u_{STC}(t)$ is

$$u_{STC}(t) = -k_1 \left| e^{\frac{r}{m}} \right|^{\frac{1}{2}} \text{sign}\left(e^{\frac{r}{m}} \right) - k_2 \int_0^t \text{sign}(e^{\frac{r}{m}}) d\tau \tag{23}$$

where k_1, k_2, r, and m are positive constants.

The stability proving of the proposed control law can be arranged by substituting Eqs. (22) into (18) as follows:

$$\begin{aligned}\dot{V} = s^T \dot{s} = s^T (&-M\dot{q} - Nq + u_{FOSMC}(t) - u_{STC}(t) + E - \ddot{q}_d \\ &+ \alpha D^{\mu} e(t) + \beta D^{\mu-1} e(t) + \gamma e(t)^{\frac{r}{m}})\end{aligned} \tag{24}$$

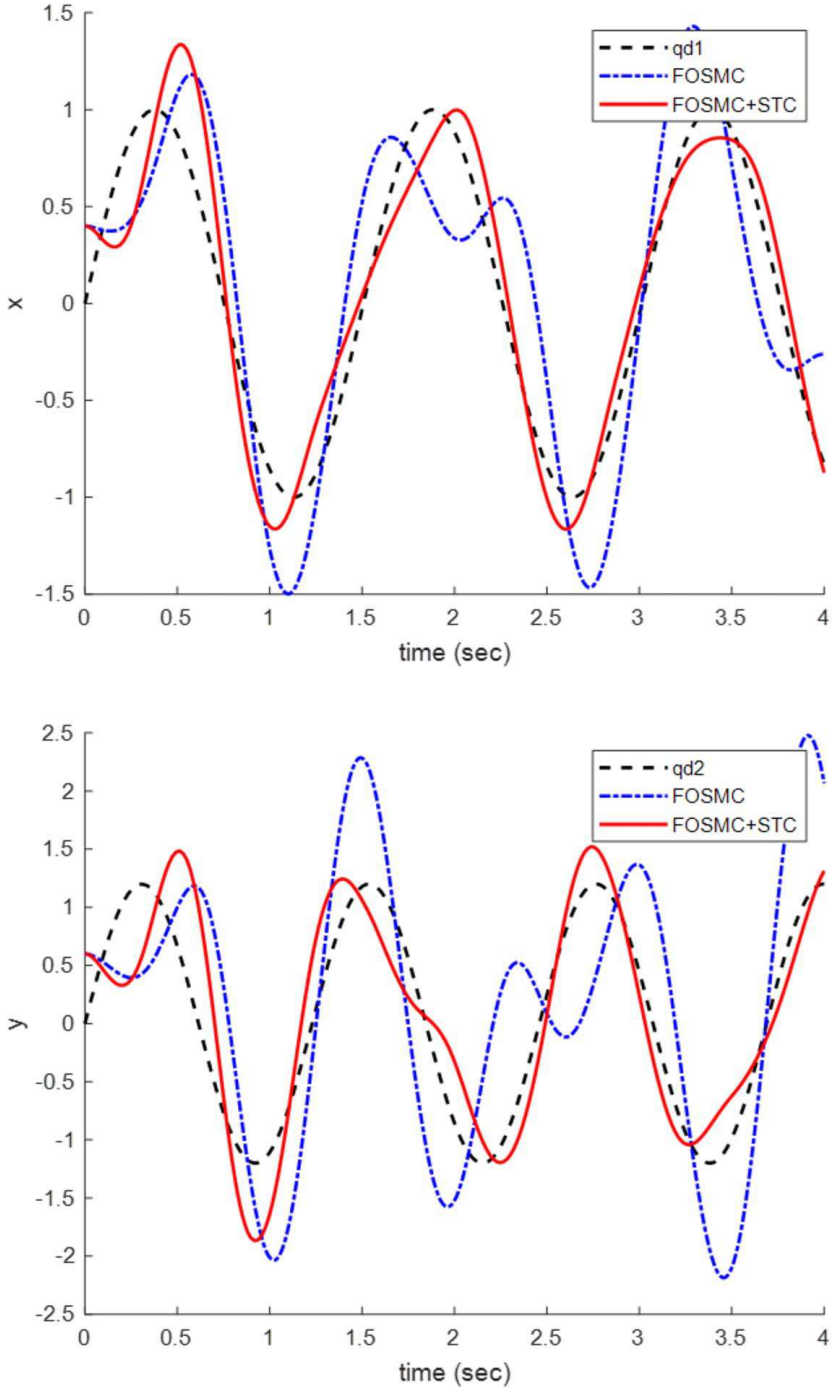

Fig. 3 Position tracking of x- and y-axes

$$\dot{V} = s^T\dot{s} = s^T(-M\dot{q} - Nq + u_{FOSMC}(t) - u_{STC}(t) + E - \ddot{q}_d - K_s s - k_1\left|e^{\frac{r}{m}}\right|^{\frac{1}{2}}\text{sign}\left(e^{\frac{r}{m}}\right) - k_2\int_0^t \text{sign}(e^{\frac{r}{m}})d\tau + E - \ddot{q}_d + \alpha D^{\mu}e(t) + \beta D^{\mu-1}e(t) + \gamma e(t)^{\frac{r}{m}}) \quad (25)$$

Simplifying Eq. (25) generates

$$\dot{V}=s^T\left(-K_s\text{sign}(s)\text{r} - k_1\left|e^{\frac{r}{m}}\right|^{\frac{1}{2}}\text{sign}\left(e^{\frac{r}{m}}\right) - k_2\int_0^t \text{sign}\left(e^{\frac{r}{m}}\right)d\tau\right) \quad (26)$$

The stability of FOSMC was proved in Sec. 3. Therefore, the main controller is stable. Also, the error was reduced by using the compound controller. This shows that the proposed controller will improve the system's stability. Therefore, Eq. (26) can be written as

$$\dot{V} = -K_s s^T\text{sign}(s) \quad (27)$$

where K_s is positive, which leads to $\dot{V} < 0$.

5 Simulation Results

The most important part of the controller design procedure is the selection of proposed controller parameters (α, β, K_s, μ, r, m, k_1, and k_2). If parameters are chosen inappropriately, the proposed control

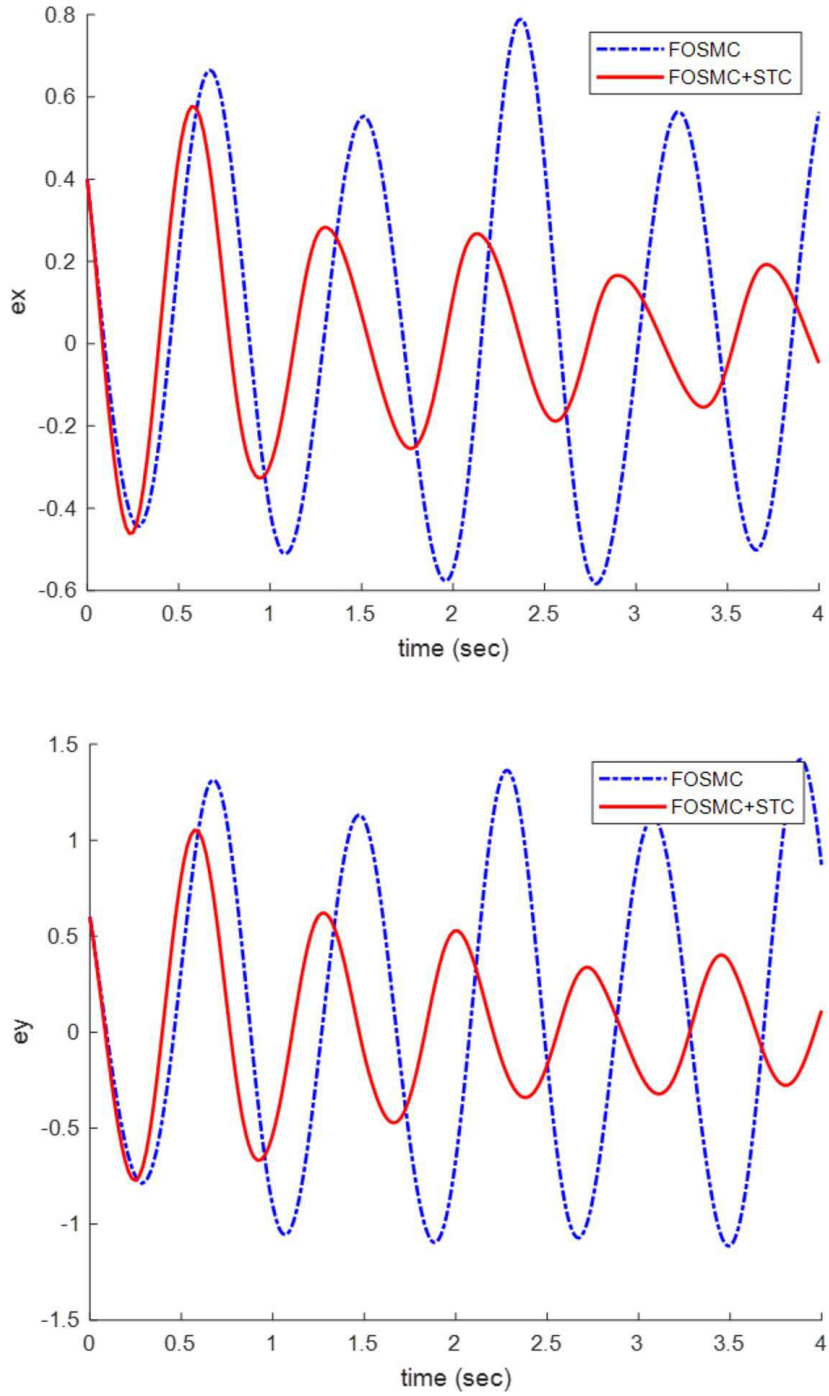

Fig. 4 Position tracking error of x- and y-axes

method cannot guarantee the desired performance, such as trajectory tracking, robustness, stability, and chattering elimination. The controller parameters are chosen based on the designer's experiences and the trial-error process. Simulation results have shown that the parameters are selected appropriately. Parameters of the fractional-order sliding mode surface are selected as $\alpha = diag\ (40,40)$, $\beta = diag\ (50,50)$, $\gamma = diag\ (60,60)$, $K_s = diag\ (10,10)$, $\mu = 2.5$, $r = 1.5$ and $m = 1.25$. The STC parameters are chosen as $k_1 = diag\ (20,20)$ and $k_2 = diag\ (20,20)$. The desired motion trajectory is determined by $q_{d1} = sin\ (4.17t)$ and $q_{d2} = 1.2\sin\ (5.11t)$. The initial values of the system are selected as follows:

$$q_1(0) = 0.5,\ \ q_2(0) = 0.5,\ \ \dot{q}_1(0) = 0 \text{ and } \dot{q}_2(0) = 0$$

The parameters of the MEMS gyroscope are selected as

$$m = 1.8 \times 10^{-7}\text{kg} \qquad k_{xy} = 12.779\ \text{N/m}$$

$$k_{xx} = 63.955\ \text{N/m} \qquad d_{xx} = 1.8 \times 10^{-6}\ \text{Ns/m}$$

$$k_{yy}95.92\ \text{N/m} \qquad d_{yy}1.8 \times 10^{-6}\ \text{Ns/m}$$

$$d_{xy} = 3.6 \times 10^{-7}\ \text{Ns/m}$$

Typically, the natural frequency of each axis of a MEMS gyroscope is in the kHz range. Thus, ω_o is selected as 1 kHz. It is suitable to choose $1\mu m$ as the reference length q_0 when the displacement range of the MEMS gyroscope in each axis is sub-micrometer level. The unknown angular velocity is assumed $\Omega_z = 100$ rad/s.

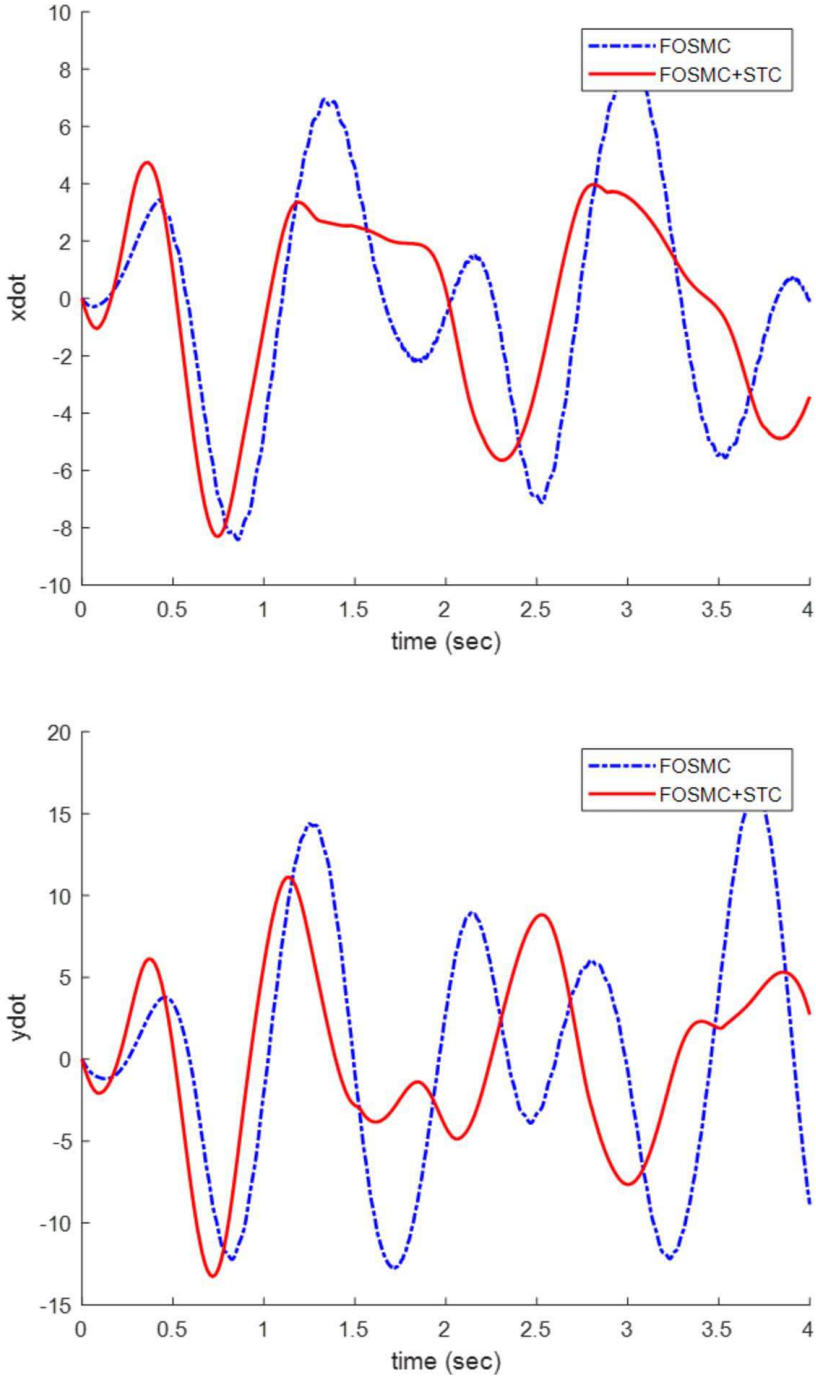

Fig. 5 Velocity of x- and y-axes

Therefore, the non-dimensional values of the MEMS gyroscope parameters are chosen as

$$\omega_x^2 = 355.3, \quad \omega_y^2 = 532.9, \quad \omega_{xy} = 70.99, \quad d_{xx} = 0.01,$$
$$d_{yy} = 0.01, \quad d_{xy} = 0.002, \quad \Omega_z = 0.1$$

Figure 3 shows position tracking of the x-axis and y-axis under FOSMC and FOSMC + STC. It can be seen clearly that tracking performance under the proposed controllers is consistent with the desired tracking of the MEMS gyroscope. Figure 4 illustrates the tracking error of the *x*-axis and *y*-axis under FOSMC and proposed control. FOSMC creates a chattering phenomenon, which by using STC is reduced. In addition, FOSMC + STC has a lower maximum overshoot and undershoot than FOSMC. Figure 5 shows the velocity of the *x*-axis and *y*-axis under FOSMC and the proposed control law. The robustness of the proposed control method was verified by applying the random noise as 0.5*randn (1,1). Figure 6 shows that the proposed control method is robust against external disturbances.

6 Conclusion

This study proposed a novel FOSMC + STC law to control a MEMS gyroscope. First, a new FOSMC is applied to control the *x*-axis and *y*-axis of a MEMS gyroscope. It has high tracking performance, but its main drawback was creating a chattering phenomenon. To solve this problem, an STC is proposed in parallel with

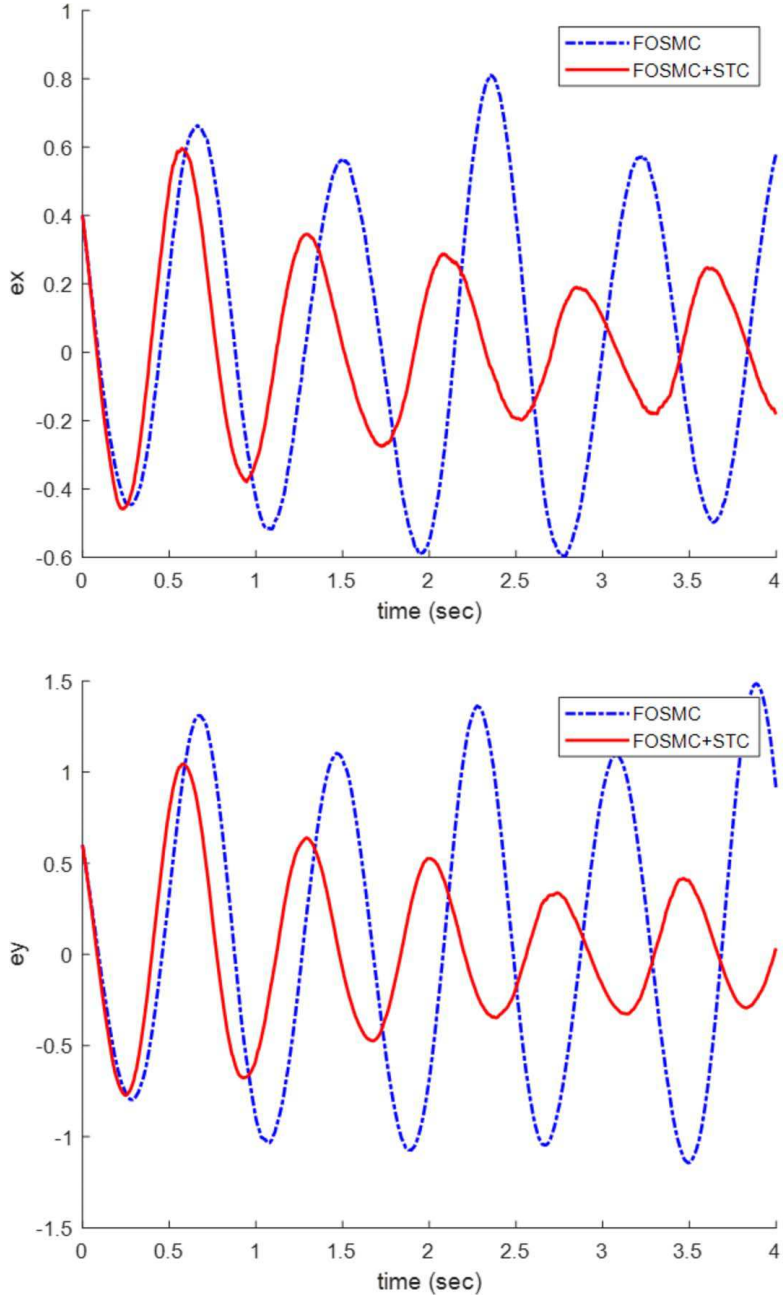

Fig. 6 Racking error under random noise

FOSMC, which continuously calculates an error value and applies a correction value. Simulated results demonstrate that the developed STC significantly reduces the chattering phenomenon. In addition, using STC, maximum overshoot and undershoot is reduced, and trajectory tracking performance improves. Simulation results thus validated the effectiveness of the proposed control strategy.

Acknowledgment

This article is based upon work supported by the National Science Foundation (Grant No. 1828010).

Conflict of Interest

There are no conflicts of interest.

Data Availability Statement

The data sets generated and supporting the findings of this article are obtainable from the corresponding author upon reasonable request.

References

[1] Yan, W., Hou, S., Fang, Y., and Fei, J., 2017, "Robust Adaptive Nonsingular Terminal Sliding Mode Control of MEMS Gyroscope Using Fuzzy-Neural-Network Compensator," Int. J. Mach. Learn. Cybern., **8**(4), pp. 1287–1299.
[2] Rahmani, M., Ghanbari, A., and Ettefagh, M. M., 2016, "Robust Adaptive Control of a Bio-inspired Robot Manipulator Using Bat Algorithm," Expert Syst. Appl., **56**, pp. 164–176.
[3] Rahmani, M., Komijani, H., Ghanbari, A., and Ettefagh, M. M., 2018, "Optimal Novel Super-Twisting PID Sliding Mode Control of a MEMS Gyroscope Based on Multi-Objective bat Algorithm," Microsyst. Technol., **24**(6), pp. 2835–2846.

[4] Yang, N., and Liu, C., 2013, "A Novel Fractional-Order Hyperchaotic System Stabilization via Fractional Sliding-Mode Control," Nonlinear Dyn., **74**(3), pp. 721–732.
[5] Gao, Z., and Liao, X., 2013, "Integral Sliding Mode Control for Fractional-Order Systems With Mismatched Uncertainties," Nonlinear Dyn., **72**(1–2), pp. 27–35.
[6] Balochian, S., 2013, "Sliding Mode Control of Fractional Order Nonlinear Differential Inclusion Systems," Evol. Syst., **4**(3), pp. 145–152.
[7] Rabah, K., Ladaci, S., and Lashab, M., 2017, "A Novel Fractional Sliding Mode Control Configuration for Synchronizing Disturbed Fractional-Order Chaotic Systems," Pramana, **89**(3), p. 46.
[8] Shah, D., and Mehta, A., 2017, "Discrete-Time Sliding Mode Controller Subject to Real-Time Fractional Delays and Packet Losses for Networked Control System," Int. J. Control Autom. Syst., **15**(6), pp. 2690–2703.
[9] Sun, G., and Ma, Z., 2017, "Practical Tracking Control of Linear Motor With Adaptive Fractional Order Terminal Sliding Mode Control," IEEE/ASME Trans. Mechatron., **22**(6), pp. 2643–2653.
[10] Wang, Y., Gu, L., Xu, Y., and Cao, X., 2016, "Practical Tracking Control of Robot Manipulators With Continuous Fractional-Order Nonsingular Terminal Sliding Mode," IEEE Trans. Ind. Electron., **63**(10), pp. 6194–6204.
[11] Aghababa, M. P., 2014, "Design of Hierarchical Terminal Sliding Mode Control Scheme for Fractional-Order Systems," ET Sci. Meas. Technol., **9**(1), pp. 122–133.
[12] Wang, H. P., Mustafa, G. I., and Tian, Y., 2018, "Model-Free Fractional-Order Sliding Mode Control for an Active Vehicle Suspension System," Adv. Eng. Softw., **115**, pp. 452–461.
[13] Kaur, S., and Narayan, S., 2018, "Fractional Order Uncertainty Estimator Based Hierarchical Sliding Mode Design for a Class of Fractional Order Non-Holonomic Chained System," ISA Trans., **77**, pp. 58–70.
[14] Khan, A., and Tyagi, A., 2017, "Fractional Order Disturbance Observer Based Adaptive Sliding Mode Synchronization of Commensurate Fractional Order Genesio-Tesi System," AEU - Int. J. Electron. Commun., **82**, pp. 346–357.
[15] Ardjal, A., Mansouri, R., and Bettayeb, M., 2018, "Fractional Sliding Mode Control of Wind Turbine for Maximum Power Point Tracking," Trans. Inst. Meas. Control, **41**(2), pp. 447–457.
[16] Guruganesh, R., Bandyopadhyay, B., Arya, H., and Singh, G. K., 2018, "Design and Hardware Implementation of Autopilot Control Laws for MAV Using Super Twisting Control," J. Intell. Rob. Syst., **90**(3–4), pp. 455–471.
[17] Jeong, C. S., Kim, J. S., and Han, S. I., 2018, "Tracking Error Constrained Super-Twisting Sliding Mode Control for Robotic Systems," Int. J. Control Autom. Syst., **16**(2), pp. 804–814.
[18] Chuei, R., Cao, Z., and Man, Z., 2017, "Super Twisting Observer Based Repetitive Control for Aperiodic Disturbance Rejection in a Brushless DC Servo Motor," Int. J. Control Autom. Syst., **15**(5), pp. 2063–2071.
[19] Zargham, F., and Mazinan, A. H., 2018, "Super-Twisting Sliding Mode Control Approach With Its Application to Wind Turbine Systems," Energy Syst., **10**(1), pp. 211–229.
[20] Zhao, Z., Gu, H., Zhang, J., and Ding, G., 2017, "Terminal Sliding Mode Control Based on Super-twisting Algorithm," J. Syst. Eng. Electron., **28**(1), pp. 145–150.
[21] Lu, K., and Xia, Y., 2014, "Finite-Time Attitude Control for Rigid Spacecraft-Based on Adaptive Super-Twisting Algorithm," IET Control. Theory Appl., **8**(15), pp. 1465–1477.
[22] Evangelista, C., Puleston, P., Valenciaga, F., and Fridman, L. M., 2012, "Lyapunov-Designed Super-twisting Sliding Mode Control for Wind Energy Conversion Optimization," IEEE Trans. Ind. Electron., **60**(2), pp. 538–545.
[23] Becerra, H. M., Hayet, J. B., and Sagüés, C., 2014, "A Single Visual-Servo Controller of Mobile Robots With Super-twisting Control," Rob. Auton. Syst., **62**(11), pp. 1623–1635.
[24] Salgado, I., Kamal, S., Bandyopadhyay, B., Chairez, I., and Fridman, L., 2016, "Control of Discrete-Time Systems Based on Recurrent Super-Twisting-Like Algorithm," ISA Trans., **64**, pp. 47–55.
[25] Rahmani, M., 2018, "MEMS Gyroscope Control Using a Novel Compound Robust Control," ISA Trans., **72**, pp. 37–43.
[26] Rahmani, M., Ghanbari, A., and Ettefagh, M. M., 2016, "Hybrid Neural Network Fraction Integral Terminal Sliding Mode Control of an Inchworm Robot Manipulator," Mech. Syst. Signal Process, **80**, pp. 117–136.
[27] Rahmani, M., Ghanbari, A., and Ettefagh, M. M., 2018, "A Novel Adaptive Neural Network Integral Sliding-Mode Control of a Biped Robot Using Bat Algorithm," J. Vib. Control, **24**(10), pp. 2045–2060.
[28] Devanshu, A., Singh, M., and Kumar, N., 2020, "Sliding Mode Control of Induction Motor Drive Based on Feedback Linearization," IETE J. Res., **66**(2), pp. 256–269.